JOURNAL OF GEOPHYSICAL RESEARCH, VOL. 97, NO. D18, PAGES 20,825–20,835, DECEMBER 20, 1992

Correlative Measurements of the Stratospheric Aerosols

R. SANTER, C. BROGNIEZ, M. HERMAN, AND S. DIALLO

Laboratoire d'Optique Atmosphérique, Université des Sciences et Technologies de Lille, Villeneuve d'Ascq, France

M. ACKERMAN

Institut d'Aéronomie Spatiale de Belgique, Brussels, Belgium

Joint experiments were organized or available during stratospheric flights of a photopolarimeter, referred to as RADIBAL (radiometer balloon). In May 1984, RADIBAL flew simultaneously with another balloon-borne experiment conducted by the Institut d'Aéronomie Spatiale de Belgique (IASB), which provides multiwavelength vertical profiles of the aerosol scattering coefficient. At this time, the El Chichon layer was observable quite directly from mountain sites. A ground-based station set up at Pic du Midi allowed an extensive description of the aerosol optical properties. The IASB and the Pic du Midi observations are consistent with the aerosol properties derived from the RADIBAL measurement analysis. The ability of RADIBAL to retrieve the vertical profile of the aerosol extinction coefficient was also demonstrated during a winter arctic campaign by comparison to Stratospheric Aerosol Measurement (SAM II) data and to airborne lidar data. As a result, RADIBAL appears to be a good candidate for in situ validations of the Stratospheric Aerosol and Gas Experiment (SAGE II) and its derived products.

1. INTRODUCTION

After the El Chichon eruption, during spring 1982, special attention was paid to the stratospheric aerosol observations. Taking advantage of the Centre National d'Etudes Spatiales (CNES) facilities to launch stratospheric balloons, we developed, at the University of Lille, a photopolarimeter, referred to as RADIBAL, designed to be set up on a gondola. A first flight in December 1983 was carefully analyzed in two articles [*Herman et al.*, 1986; *Santer et al.*, 1988]. This first flight corresponded to constant altitude measurements. Since that time, this experiment has probed the stratospheric layer on a routine basis twice a year, both during ascent and descent of the balloon. Our first goal is to adapt our previous inversion scheme to the balloon trajectory including ascent and descent.

Photopolarimetric observations have also been made simultaneously with other ground, aircraft, balloons, and satellite-based experiments. First, in May 1984 a ground-based station was set up at l'Observatoire du Pic du Midi. From this 3000-m elevation site and with a stratosphere highly polluted by El Chichon, the stratospheric layer was quite directly accessible: the tropospheric contribution should be residual compared to the stratospheric component. During the same campaign, photography at limb was performed as reported by *Ackerman et al.* [1981].

Finally, the participation of radiometer balloon (RADIBAL) in the Chemistry of the Polar Stratosphere (CHEOPS) experiment in January 1988 allowed us to compare our measurements to Stratospheric Aerosol Measurement (SAM II) data and to the NASA lidar data which simultaneously flew on board a DC8. The intercomparison of the different techniques describing the stratospheric aerosol will be achieved.

Paper number 92JD02013.
0148-0227/92/92JD-02013$05.00

2. PHOTOMETRIC EXPERIMENT RADIBAL

2.1. *Principle of the Experiment and Expression of the Signal*

A detailed description of the instrument is given in *Herman et al.* [1986] and is briefly recalled here. Figure 1 from *Santer et al.* [1988] is needed for the following discussion. The photopolarimeter is set up horizontally on the gondola of a stratospheric balloon, which is rotated at a uniform rate of 1 rpm. Every minute, the instrument measures the radiance and the degree of polarization of the sky light in horizontal directions at three wavelengths: 850, 1350, and 1650 nm. At sunset or at sunrise the radiometer scans the full range of scattering angles between 0 and 180°. The horizontal stability of the gondola is verified by an inclinometer, while its azimuth is measured by a two-axis magnetometer. The solar angles are computed from the location of the balloon recorded every 20 s.

We now propose a simple formulation of the signal. The radiance is converted into reflectance ρ expressed in the primary approximation versus the scattering angle Θ, as already proposed in *Santer et al.* [1988] by

$$\rho(\Theta) = \frac{t(h_s, \Theta)}{4} [\delta_a^s p_a + \delta_R^s p_R + (\delta_a^s + \delta_R^s) 2\rho_G \sin h_s] \quad (1)$$

The subscripts a and R stand for aerosols and Rayleigh, respectively, and δ^s is the slant optical thickness. Primary scattering from the direct solar beam is proportional to the phase function p. The last term corresponds to primary scattering from light reflected by the Earth-troposphere system that is described by its reflectance ρ_G. This term depends upon the solar elevation h_s. The relevant isotropic contamination is proportional to the total optical thickness. The transmission term t describes (1) the attenuation of the direct solar beam to reach an elementary scattering element within the field of view (FOV) of the instrument and (2) the

attenuation of the diffuse light. In (1), we suppose the aerosols are constant in nature with altitude and uniformly mixed with the molecules. This last assumption allows us to factorize the transmission term which an average describes the mean attenuation of the solar beam and of the diffuse light. *Santer et al.* [1988] showed that this formulation is still quite valid if the mixture between Rayleigh and aerosols is no longer constant.

The polarization ratio

$$P = \frac{\delta_a p_a P_a + \delta_R p_R P_R}{\delta_a p_a + \delta_R p_R + (\delta_a + \delta_R) 2\rho_G \sin h_s} \quad (2)$$

depends upon the degree of polarization of the aerosol P_a and of the molecules P_R. In (2), the transmission term, which affects the total reflectance and the polarized reflectance in the same way, is simplified, and the tropospheric contamination is expected to be unpolarized.

Equations (1) and (2) correspond to the primary scattering approximation. *Santer et al.* [1988], using a Monte Carlo code to include multiple scattering, proved the validity of this approximation.

2.2. *Computation of the Signal*

At a given level z, we characterize the aerosols by their size distribution $n(r)$, their refractive index, and their concentration.

The size distribution is described by a lognormal law

$$n(r) = \frac{1}{r\sqrt{2\pi}\,\sigma} \exp\left(-\frac{\ln^2 r/r_m}{2\sigma^2}\right) \quad (3)$$

with two flexible parameters: the mean radius r_m and the variance σ.

In standard conditions (i.e., except for polar stratospheric clouds (PSC)), the aerosols are treated as hydrated sulfuric aerosol particles, and the relevant value of the refractive index is chosen. The aerosol abundance is proportional to the scattering coefficient σ_a integrated here with altitude, in respect to the geometry of the experiment, to get the slant optical thickness δ_a^s. Finally, at a given altitude z, the aerosols are described by r_m, σ, and δ_a^s.

The two other contributors to the signal are Rayleigh scattering, which is computed from the barometric pressure at the balloon level and from the seasonal value of the temperature, and the scattering of the diffuse tropospheric light. The determination of the tropospheric reflectance ρ_G requires special attention. We first need to point out that the influence of this term is reduced by working around sunset or sunrise. A method to get ρ_G is described in *Santer et al.* [1988]. The balloon is maintained at the same altitude long enough to observe the effects of the ground contribution when the solar elevation h_s varies. The aerosols being identical, one can derive ρ_G through

$$\frac{1}{P} = \frac{1}{P^0}\{1 + C\rho_G \sin h_s\} \quad (4)$$

where P^0 is the polarization ratio for $h_s = 0$ and C is a constant.

This strategy was conducted for sunrise flights with an overnight ascent and a constant ceiling after the sunrise, providing the required h_s variations, before the descent, for which the gondola is quite stable, could start. For sunset flights, we tried to maintain the altitude of the balloon at the end of the descent to wait for the sunset. Unfortunately, it is technically difficult to stabilize the balloon. An alternative is to take advantage of available measurements during both the ascent and the descent at the same altitude (i.e., with the same aerosols) for different solar elevations. Since the gondola is much more stable during the descent, we will invert the signal for a set of ground reflectance values. Then we assume that the aerosols are identical during the ascent at the same altitude, and we compare the measurements to the computation achieved with the inverse model. The fit provides suitable values of the ground reflectances at the two wavelengths 850 and 1650 nm.

2.3. *The Inversion Scheme*

Four basic steps are involved in the inversion.

1. The aerosol slant optical thickness δ_a^s is derived from the calibrated reflectance measurement at $\lambda = 1650$ nm and for $\Theta = 30°$. This angle is selected because the phase function for that angle is quite independent of the nature of the aerosols. Moreover, Rayleigh scattering and tropospheric light influences are small in the forward direction. The wavelength $\lambda = 1650$ nm is selected to reduce molecular scattering and because the aerosol slant optical thickness is much weaker at this wavelength, so that the δ_a^s retrieval from the reflectance is more accurate. Therefore, if we only consider the aerosol contribution, we can express the reflectance as

$$\rho(30°, h_s = 0°) = \frac{\delta_a^s e^{-\delta_a^s}}{4} p_a \quad (5)$$

at sunrise, or as

$$\rho(30°, h_s > 5°) = (1 - e^{-\delta_a^s}) \frac{p_a}{4} \quad (6)$$

when the sun is high enough above the horizon (i.e., $h_s > 5°$). In these two cases, optical thicknesses of the order of 1 raises a problem. Such values can be found in lower altitudes at $\lambda = 850$ nm. Conversely, at $\lambda = 1650$ nm, the sensitivity of ρ to δ_a^s is suitable with decreasing optical thicknesses when the wavelength increases.

2. We now consider the degree of polarization at $\Theta = 90°$ and $\lambda = 1650$ nm. The value of $\Theta = 90°$ corresponds to the maximum of polarization. The behavior of P versus the particle size is quite simple: it starts from the Rayleigh regime and decreases when the particle size increases. For a set of σ, the retrieval of the measurement is done via (2) using a dichotomy method on r_m. Since at $\lambda = 1650$ nm the Rayleigh scattering contribution is weak, the computation of the degree of polarization via (2) is not critically sensitive to δ_a^s. A standard value of p_a in the δ_a^s retrieval already provides a good guess for (2). The two first steps are iterated one time. The final result is a series of values of (r_m, δ_a^{1650}) for a selected set of σ of 26 values ranging between 0.02 and 1.

3. For each solution, the degree of polarization at $\Theta = 90°$ for $\lambda = 850$ nm is computed by using (2) and is compared to the corresponding measurement. When σ decreases, the wavelength dependence of the phase matrix is more impor-

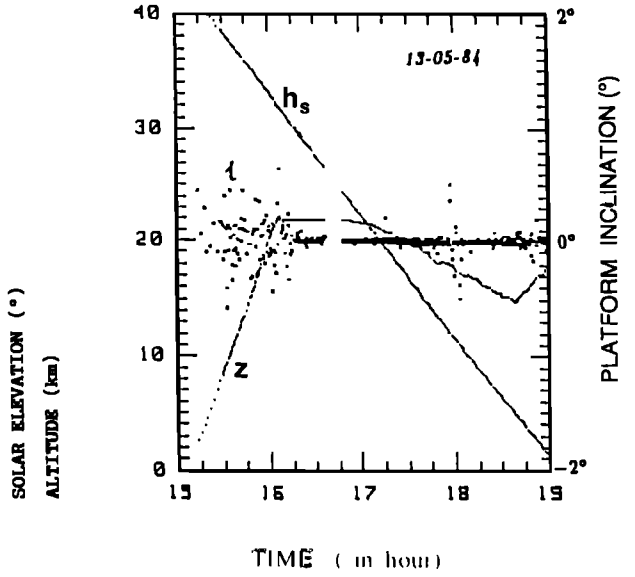

Fig. 1. Main characteristics of the May 13, 1984, flight. Balloon altitude (z in kilometers), solar elevation (h_s in degrees, left scale), and platform inclination (in degrees, right scale) are plotted versus UT in hours.

tant, so the computed polarization ratio P_a increases continuously with decreasing σ, and the measurement retrieval provides a unique solution.

4. Finally, for a complete scan, we compare the measurements at 850 and 1650 nm both for the reflectance and for the degree of polarization to the respective computations using (1) or (2). This procedure is achieved mainly to confirm the aerosol retrieval when the layer homogeneity is sufficient.

2.4. *Example of Results*

We apply our inversion scheme to the May 13, 1984, flight launched from the CNES balloon center at Aire sur l'Adour (43.°4N, 0.°15E). Figure 1 gives the main characteristics of this flight versus UT. The vertical profile corresponds to a rapid ascent with instability of the gondola as indicated by the inclinometer data. The balloon was stabilized during one hour at 22-km altitude. Then the descent was stopped at 15 km, and an attempt was made to stabilize the balloon and wait for sunset, but the balloon rose slightly. The balloon reached 3 times the altitude of 17 km. Depolarization by tropospheric light corresponded to $\rho_G = 0.30$ at 850 nm and to 0.27 at 1650 nm.

As an example, the retrieved diagrams obtained after inversion with $r_m = 0.22$ μm and $\sigma = 0.36$ (i.e., $r_{\text{eff}} = 0.30$ μm and $v_{\text{eff}} = 0.14$) are compared with the measurements in Figure 2 for $z = 18$ km. The reflectances measured at 1650 nm are more than 10 times larger than the reflectances corresponding to the molecular scattering, and the restitution of the signal is quite perfect. At 1650 nm, a slight asymmetry appears in the backward region. The restitution of the polarization is also satisfying. At 850 nm, the neutral point around $\Theta = 140°$ is characteristic of the sulfuric refractive index. Figure 3 reports the vertical distribution of the retrieved aerosol slant optical thicknesses at the two wavelengths. Between 14 and 18 km, measurements correspond both to the descent (crosses) and to the small ascent (stars) at the end of the flight. The same altitudes are probed at different solar elevations, corresponding to different effects of the tropospheric light, and the good agreement between the two data sets indicates that ρ_G was correctly estimated. The ratio between the optical thicknesses at the two wavelengths is quite independent of the altitude, with an Angstrom coefficient around 2.

The retrieved vertical profile follows almost an exponential law

$$\delta_a(z) = \delta_a(z_0)e^{-(z-z_0)/H_a} \tag{7}$$

where $H_a \approx 3.7$ km.

In this case, the extinction coefficient is related to the slant optical thickness by

$$\sigma_a = \frac{\delta_a}{\sqrt{\pi R H_a/2}} \approx \frac{\delta_a}{200} \tag{8}$$

where R is the Earth's radius. A typical value of σ_a (850 nm) at 15 km is then 5×10^{-3} km^{-1}. Finally, Figure 4 gives the vertical profile of the effective radius and of the effective variance as defined by *Hansen and Travis* [1974]:

$$r_{\text{eff}} = \int_0^\infty r\pi r^2 n(r)\, dr \Big/ \int_0^\infty \pi r^2 n(r)\, dr \tag{9}$$

$$v_{\text{eff}} = \int_0^\infty (r - r_{\text{eff}})^2 r^2 n(r)\, dr / r_{\text{eff}}^2 \int_0^\infty r^2 n(r)\, dr \tag{10}$$

The characteristics of the particles are quite stable with latitude, with $r_{\text{eff}} \approx 0.32$ μm for $v_{\text{eff}} \approx 0.15$; one can observe only a slight decrease of these parameters when the altitude is increasing.

3. Comparison to Other Observations

We will verify, through comparisons, the ability for RADIBAL inverted models to correctly describe the aerosol layer, by means of the extinction coefficient profiles, and the optical properties of the medium, such as the phase function or the spectral dependence of the extinction coefficient. The preliminary point is to ensure that the joint experiments probe as close as possible the same air mass or air masses proved to be identical. We had this opportunity two times. First during May 1984, with ground-based and balloon experiments, then during January 1988, with satellite and airborne experiments.

3.1. *May 1984 Campaign*

3.1.1. *The ground-based measurements.* L'Observatoire du Pic du Midi is located in the Pyrenées, at 3000-m elevation, 100 km south from Aire sur l'Adour. During the first flight of RADIBAL, in December 1983, the measurements indicated a vertical aerosol optical thickness of 0.10 at 850 nm for the stratospheric layer. We could then expect a significant stratospheric contribution to total extinction in ground-based measurements, so a ground-based station with passive optical measurements was set up from May 4 to May 13, 1984.

3.1.1.1. *Optical thickness measurements:* Two sun radiometers were used. The first, using a silicon detector, had

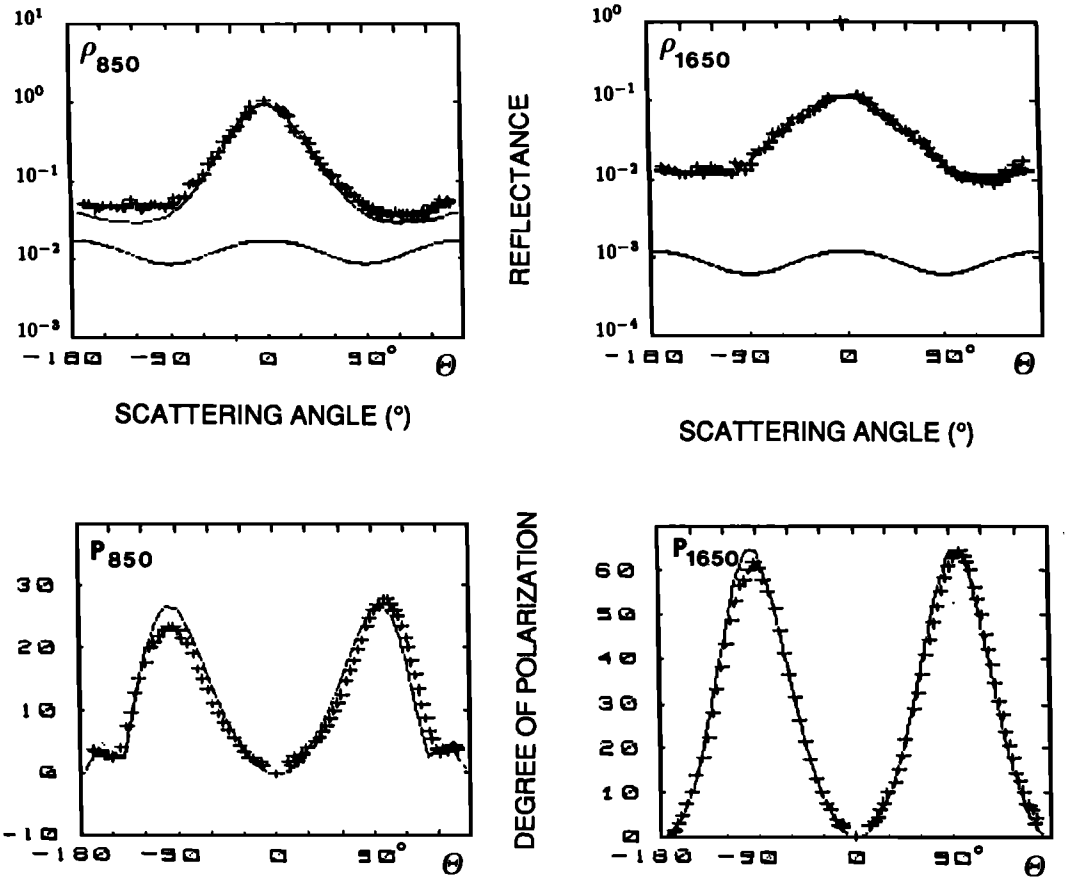

Fig. 2. Restitution of a sequence of measurements taken on May 13, 1984, at z = 18 km during descent with the inverted model deduced from the polarization measurements at $\Theta = 90°$ (r_m = 0.22 μm for σ = 0.36). The measurements (crosses) are plotted versus the scattering angle (negative values correspond to the half space containing the north). For the two wavelengths, we plotted the reflectance (in log scale) and the degree of polarization (in percent). The computed signals are shown by solid line. For the reflectances, we added (lower curves) the intrinsic molecular reflectance.

five bands in the range 450–860 nm (445, 525, 600, 678, and 850 nm), while the second used a cooled PbS detector with similar bands (445, 550, 648, and 865 nm) plus the three atmospheric windows in the middle infrared at 1050, 1650, and 2200 nm. The two radiometers were calibrated using the Langley-Bouguer technique. The measurements provided the aerosol vertical optical thicknesses. The Rayleigh optical thicknesses were derived from barometric pressure measurements, and the ozone optical thicknesses in the Chappuis band were computed from the climatologic ozone content.

Figure 5 is a plot of the vertical aerosol optical thickness versus time at λ = 525 nm for the four dates available. The aerosol optical thickness varies from 0.12 to 0.20. Since the stratospheric layer is usually quite stable with time, these variations are probably due to the variable contribution of the troposphere. Figure 6 reports the spectral variations of the optical thicknesses observed at 1000 UT for the four dates. The main feature is the quite null spectral dependence in the visible below 600 nm if we account for the measurement uncertainties. This behavior is common to the two instruments despite the fact that a systematic bias appears between them. The cooled PbS detector may be not correctly stabilized in temperature, especially in the early morning, when low temperatures were recorded. In the

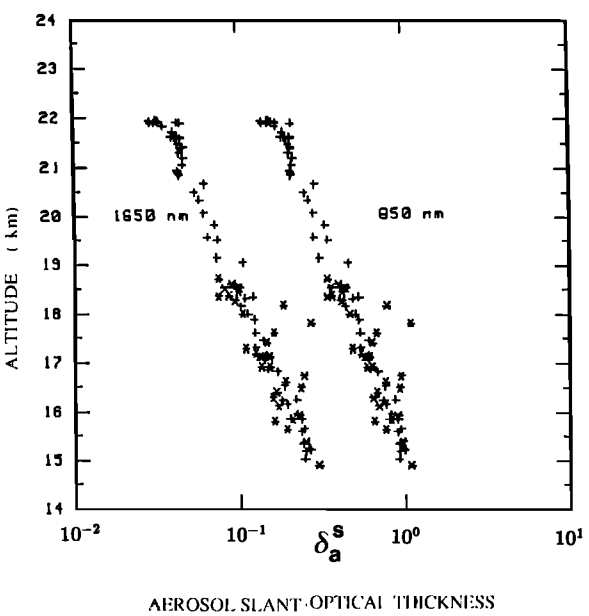

Fig. 3. Vertical profiles at the two wavelengths of the aerosol slant optical thicknesses on May 13, 1984. Crosses stand for the descent, and stars for the ascent.

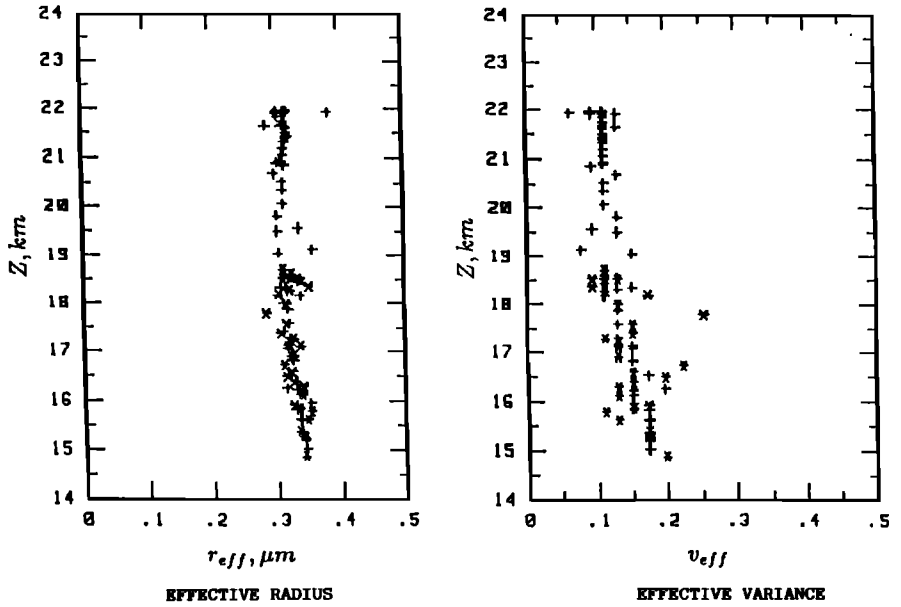

Fig. 4. Effective radius and effective variance of the aerosols versus altitude on May 13, 1984. Symbols are the same as in Figure 3.

middle infrared the optical thicknesses decrease sharply. Nevertheless, we need to be careful in the quantitative use of these data, first, in regard to the small values of δ_a^v of the order of the calibration error. Second, the measurements may be slightly affected at 1650 nm and 2200 nm by the water vapor absorption which was not corrected, assuming a negligible water vapor content above the Pic du Midi.

3.1.1.2. *Aureole measurements:* The aureole is measured at 850 nm in the almucantar region, i.e., the same zenith angle for sun and view. After pointing at the sun, the 1° FOV radiometer is rotated in azimuth. Table 1 reports the data and the time of the measurements plus the air mass and the derived aerosol vertical optical thickness at 850 nm during May 1984. All the measurements are normalized assuming a standard value of 5 for the phase function at Θ = 30°. The iterative scheme developed by *Weinman et al.* [1975] was applied to correct for multiple scattering. For these conditions, Figure 7 is a plot of the measurements listed in Table 1. The lower curve corresponds to the first set, and all curves are translated to each other by a constant.

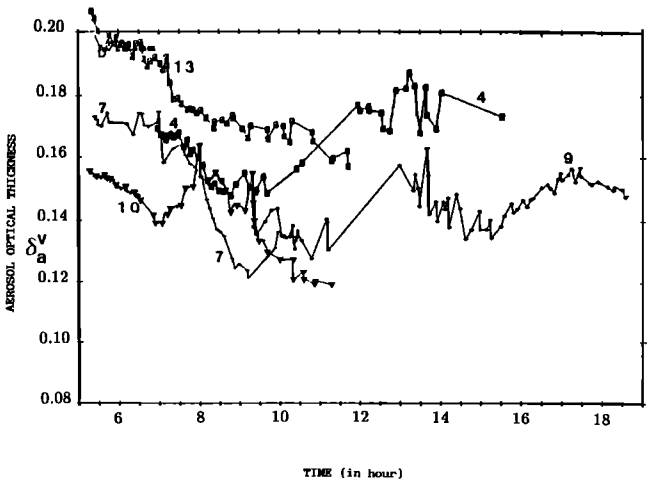

Fig. 5. Aerosol vertical optical thicknesses, measured at λ = 525 nm, from L'Observatoire du Pic du Midi in May 1984 versus UT. The day number is labeled on each curve. May 4, solid squares; May 7, crosses; May 9, diamonds; May 10, triangles; and May 13, open squares.

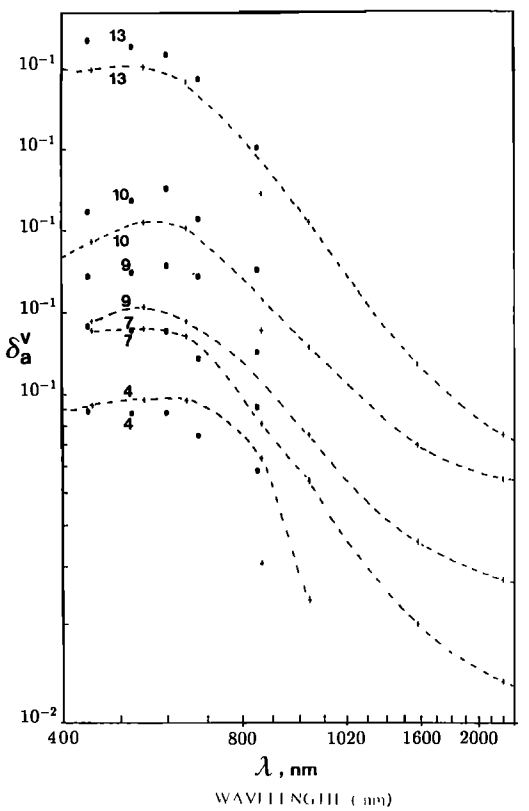

Fig. 6. Aerosol vertical optical thicknesses taken on the same dates as in Figure 5, versus wavelength at 1000 UT. The vertical scale is given for May 4, and the curves are uniformly translated for each day. Crosses correspond to the silicon detector, and dots to the PbS detector. Dashed lines correspond to an approximate fit of the PbS measurements.

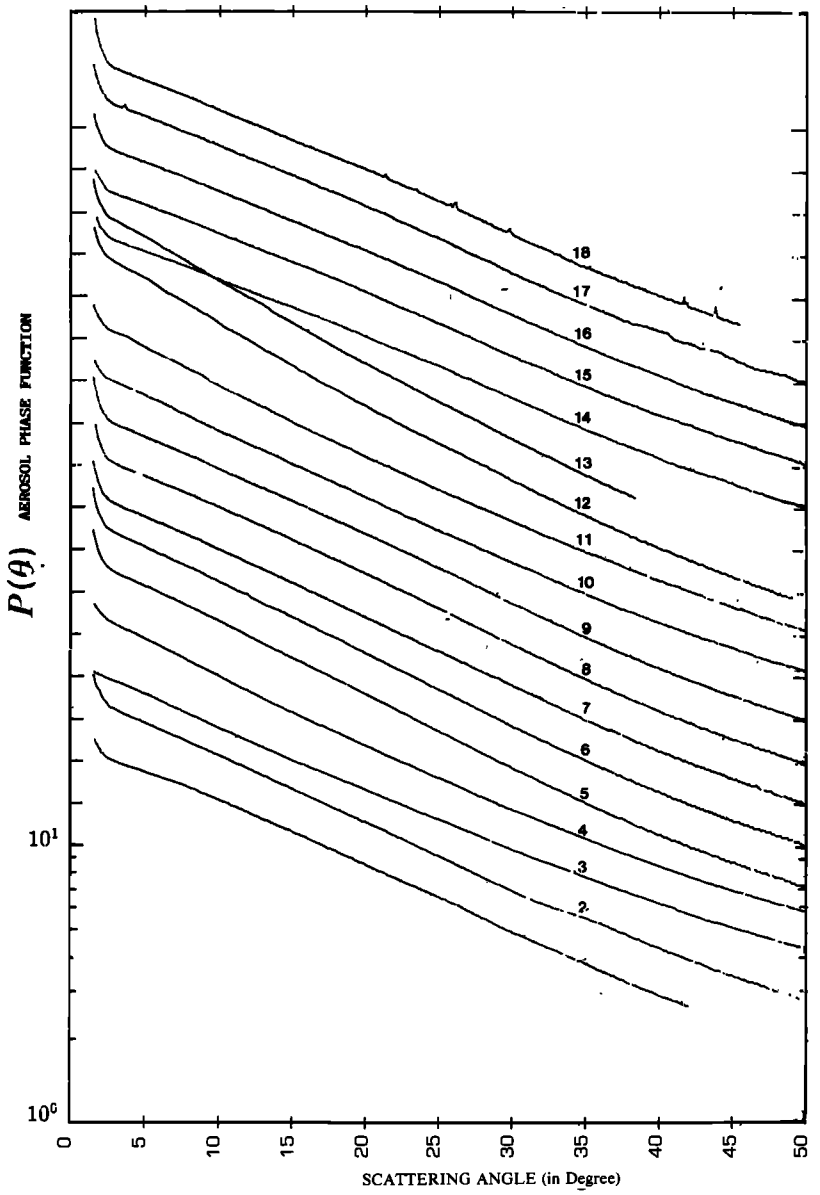

Fig. 7. Aerosol phase functions deduced from the aureole measurements listed in Table 1. The vertical log scale is given for the first measurements. All sets are uniformly translated by a constant factor: the upper tick marks correspond to the phase function, equal to 10 for the last aureole measurements of Table 1.

All the measurements are quite identical except 12 and 13, which present a sharper forward peak correlated to an increase of the optical thickness. Additional large tropospheric aerosols are probably involved in the increase of the forward scattering.

3.1.1.3. *Polarization measurements:* A twin photopolarimeter of the stratospheric instrument was used for scanning in the principal plane. Limited results are reported in Figure 8. The slight decrease of the maximum of the polarization with time corresponds to the depolarization by the ground, since this effect is known to be proportional to sin (h_s) (equation (2)).

3.1.1.4. *Inversion of the measurements:* Different strategies can be conducted in the analysis of the ground-based measurements. *Devaux et al.* [1989] suggest combining an inversion method of the optical thicknesses as proposed by *King et al.* [1978] with an inversion method of the aureola as suggested by *Santer and Herman* [1983]. When dealing with tropospheric aerosols, the deduced aerosol size distribution is quite insensitive to the particle refractive index. The polarization measurements are then used to determine this refractive index.

The goal here is to check the RADIBAL performances. The analysis is then based on the polarization measurements with a scheme quite identical to that of the balloon experiment. We also combine the degrees of polarization at $\Theta = 90°$ for the two wavelengths to derive the two flexible parameters of the lognormal size distribution. Simply, the computation of the signal suits the experimental conditions. The transfer equation, numerically solved by using the successive orders of scattering code [*Deuzé et al.*, 1989], is used to include the multiple scattering. Moreover, the measured aerosol vertical optical thicknesses are used as inputs.

The inversion scheme was applied to the set of measure-

ments obtained on May 13 at 0520 UT. The measured optical thickness is δ_a^v (850 nm) = 0.072. We first assumed that the signal had a stratospheric origin, and the refractive index of the particles was then supposed to be 1.45. We then got r_m = 0.33 μm and σ = 0.35 (i.e., r_{eff} = 0.45 μm and v_{eff} = 0.13). Then with this model, we simulated the various measurements. The measurements are compared with the computations (dashed lines) in Figure 9. The measured polarization is quite correctly retrieved at the two wavelengths (Figures 9*a* and 9*b*). In the forward scattering, the model underestimates the aureola measurements in the first 10° (Figure 9*c*). For the vertical optical thicknesses, the model predicts an unobserved decrease in the visible toward the blue. In the infrared, due to large uncertainties in the measurements, the comparison is unrealizable (Figure 9*d*).

A second inversion was made in an attempt to correct for the tropospheric contribution. We already pointed out that the variations of the observed optical thicknesses may originate from the troposphere. According to the World Meteorological Organization, a standard continental model with δ_a (550 nm) = 0.02 occupies the troposphere above the boundary layer. We then corrected the signal from this tropospheric contamination. The inversion of the polarization gives slightly smaller particles, with r_m = 0.32 μm and σ = 0.34 (i.e., with r_{eff} = 0.43 μm and v_{eff} = 0.12). The ground-based measurements were simulated again with this two-layer model. The results are reported in Figure 9 (solid lines). We can observe that the aureole measurements are now correctly retrieved and, in the same way, that the flat spectral behavior of the optical thicknesses in the visible range is correctly fitted.

3.1.1.5. *Comparison with the RADIBAL results:* We already saw (equations (7) and (8)) how to convert approximately the slant optical thicknesses measured by RADIBAL into extinction coefficients all along the RADIBAL vertical profile, i.e., above 15 km. From radiosondes, we know that the tropopause was located at 8 km. If we suppose that the aerosol vertical distribution is exponential with the scale height equal to 3.7 km derived from Figure 3, we get δ_a^v (850 nm) = 0.057, which is quite consistent with the ground-based measurement, i.e., 0.059, obtained when removing the tropospheric background (Figure 6).

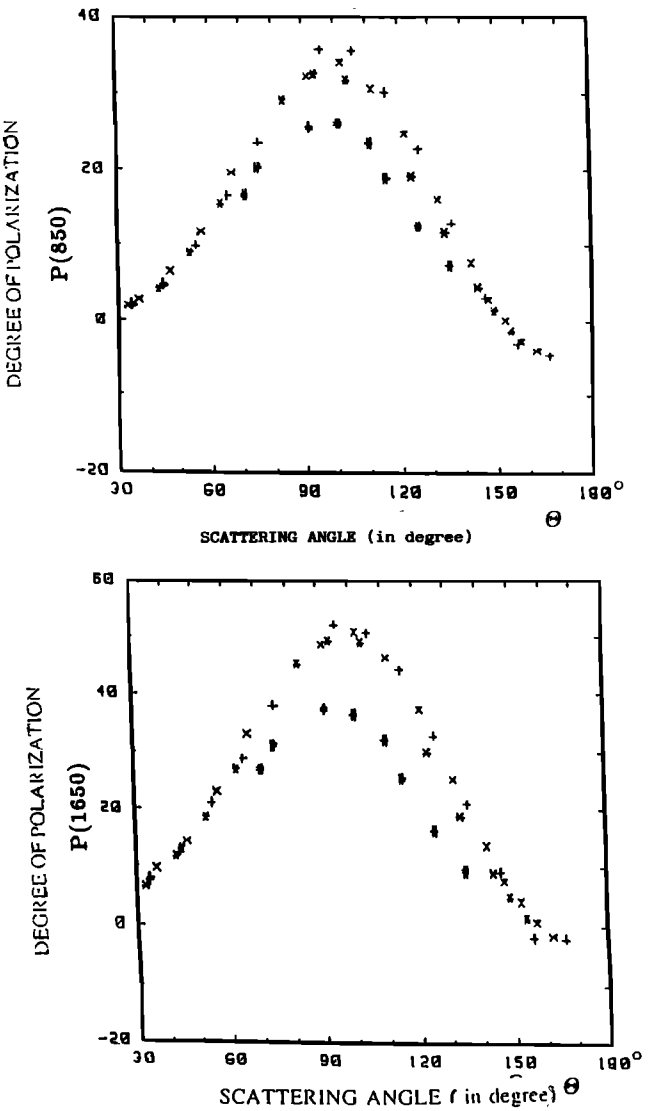

Fig. 8. Ground-based polarization measurements from Le Pic du Midi on May 10 at 0750 UT (double-cross symbol), May 13 at 0520 UT (plus signs), May 13 at 0600 UT (crosses), and May 13 at 0630 UT (asterisks) for the two wavelengths 850 nm and 1650 nm. Measurements correspond to the principal plane and are plotted versus the scattering angle.

TABLE 1. Aureole Measurements Reported for the Date and Hour of the Start of Measurements, Viewed Air Mass, Aerosol Vertical Optical Thickness, and Phase Function at 2°

	Date in May	Hour	m	δ_a^v	$P(2°)$
1	4	0810	1.7	0.048	26.5
2	4	1318	1.18	0.068	35.9
3	7	0521	8	0.055	21.5
4	7	0627	3	0.055	25.5
5	9	0950	1.2	0.063	29
6	9	1435	1.4	0.048	29
7	9	1506	1.6	0.048	26.2
8	9	1544	1.7	0.044	26.5
9	9	1624	2.5	0.043	25.7
10	10	0639	2.4	0.043	24.5
11	10	0714	2.1	0.053	27
12	10	0821	1.5	0.073	34.5
13	10	0913	1.7	0.078	35
14	13	0700	2.25	0.068	20
15	13	0741	1.75	0.063	21.6
16	13	0832	1.51	0.058	22.2
17	13	0911	1.35	0.058	23
18	13	0951	1.2	0.063	23

In terms of size distribution, we averaged the r_{eff} and v_{eff} profiles, weighted by the slant optical thickness, over the balloon vertical profile and got r_m = 0.25 μm and σ = 0.36 (i.e., r_{eff} = 0.34 μm and v_{eff} = 0.14). From the ground-based measurements, as seen previously, we derived larger particles with r_m = 0.32 μm and σ = 0.34 (i.e., r_{eff} = 0.43 μm and v_{eff} = 0.12). To interpret this discrepancy, we can point out that the layer probed by RADIBAL only represents 40% of the stratospheric layer, and that a general trend of the particle size is to increase toward lower altitudes. On the other hand, from the ground-based measurements, we only introduced the troposphere background. Figure 5, where the measured optical thicknesses were drawn, indicated that May 13 was the most turbid day. If the tropospheric con-

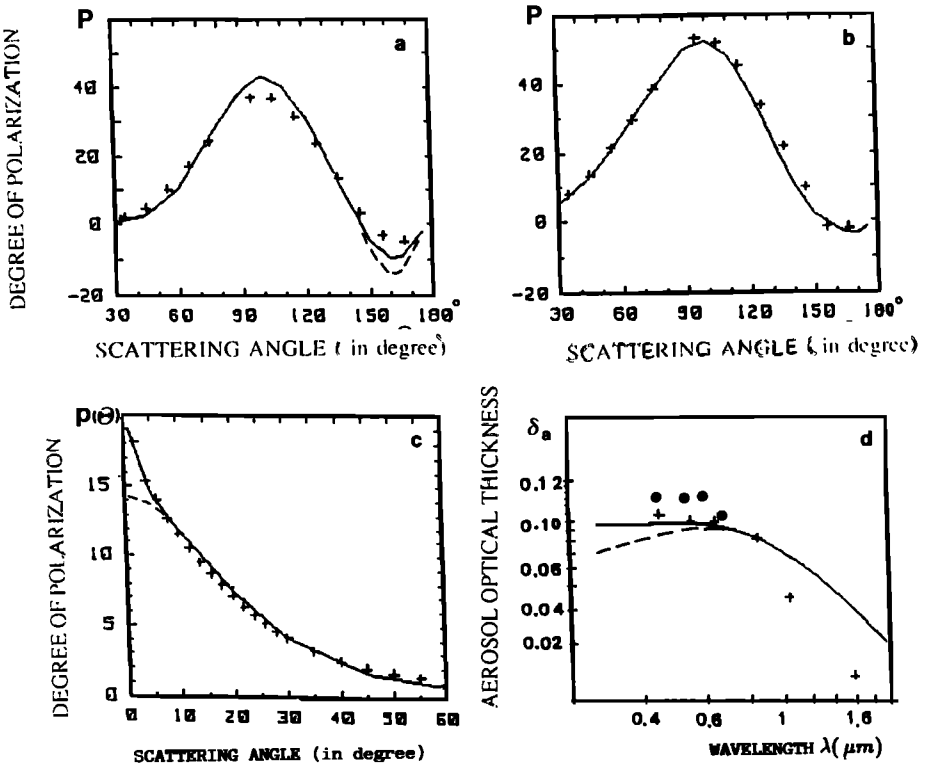

Fig. 9. Restitution of the ground-based measurements on May 13 with the aerosol model inverted from the polarization measurements at the two wavelengths for $\Theta = 90°$. Percent polarization measurements (crosses) are drawn versus the scattering angle at (*a*) $\lambda = 850$ nm and (*b*) $\lambda = 1650$ nm. (*c*) The aerosol phase function (crosses) plotted versus the scattering angle. (*d*) Multispectral measurements of the aerosol optical thicknesses graphed for the Si detector (dots) and for the Pbs detector (crosses). Dashed lines are computed for a uniform aerosol layer with $r_m = 0.33$ μm and $\sigma = 0.35$. Solid lines correspond to a two-layer atmosphere with a standard tropospheric component and a stratospheric layer with $r_m = 0.32$ μm and $\sigma = 0.34$.

tamination is more important than supposed, then the ground-based measurements should provide smaller particles for the stratosphere.

3.1.2. *The limb experiment.* A companion balloon equipped by the Institut d'Aéronomie Spatiale de Belgique (IASB) was flown during the same period. In the IASB experiment, images of the solar disk are taken from the gondola of a stratospheric balloon stabilized above the stratospheric layer at 30-km height. Three Hasselblad cameras are used, equipped with three filters at 440, 650, and 840 nm. A first image of the sun is taken when the sun is high above the horizon. This reference image corresponds to a transmission equal to 1. Then we have a series of pictures after the sunset. For each image, the sun is viewed below the horizon at different tangent altitudes. The film sensitivity is measured using calibrated transmission plates, and the experiment is self-calibrated when working in transmission on the sun. In order to analyze the diffuse light, an absolute calibration is realized on the moon, which presents the suitable radiance, when it is high above the horizon. The film is digitalized, and the result is a series of transmission factors for sun-to-balloon paths at different tangent altitudes below the gondola.

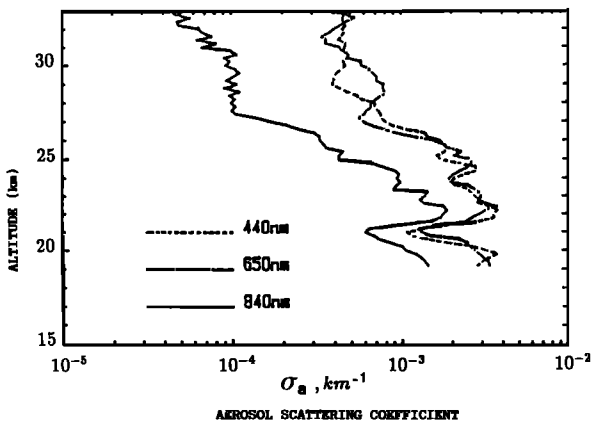

Fig. 10. Vertical profiles of multispectral aerosol extinction coefficients derived from the limb photography.

An onion peel method is then applied to derive the vertical profile of the extinction coefficient [*Ackerman et al.*, 1981]. The results, reported in Figure 10 after removing the Rayleigh contribution, indicate an inhomogeneous structure above the Junge layer. The blue and red vertical profiles are quite identical, and we retrieve the null spectral dependence of the aerosol optical thicknesses measured from Le Pic du Midi.

The extinction coefficients at 850 nm are converted into slant optical thicknesses with

$$\delta_a(z) = \sqrt{R/2} \int_z^\infty \frac{\sigma_{a(z')}}{\sqrt{z' - z}} dz' \qquad (11)$$

The results, plotted in Figure 11, compare favorably to the RADIBAL measurements. The ceiling for RADIBAL at 22

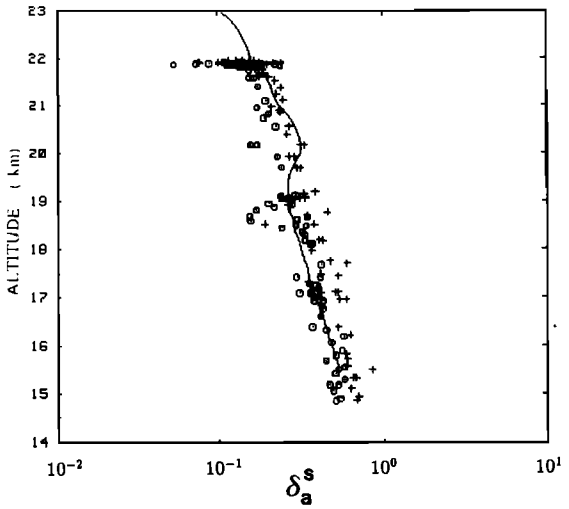

Fig. 11. Comparison of the aerosol slant optical thicknesses at 850 nm (open circles correspond to negative scattering angle, and crosses to positive scattering angle), versus altitude, measured by RADIBAL and the limb experiment (solid line).

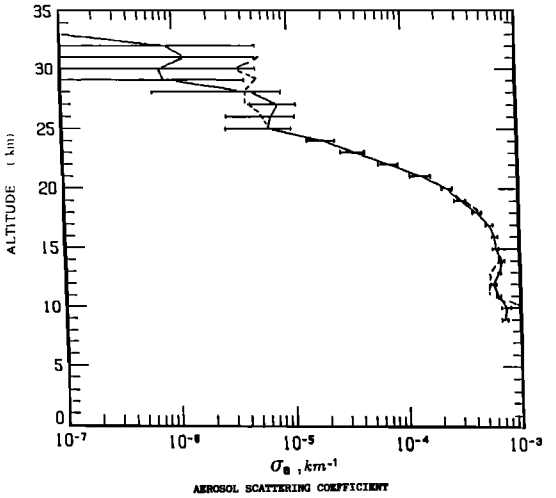

Fig. 13. Vertical profile at λ = 1020 nm of the aerosol extinction coefficient as measured by SAM II on January 28, 1988. The solid line is for the event located at (69.9N, 13.8E) with error bars, and the dashed line is for (69.9N, 28.33E).

km gives an idea of the measurement dispersion, and the IABS measurement curve fits the RADIBAL-derived slant optical thicknesses.

3.2. *January 1988 Campaign*

RADIBAL was flown from Kiruna, Sweden, during the CHEOPS experiment on January 28, 1988. On this day a set of data was acquired by SAM II at an approximate latitude of 70°N in the range of longitude (3°W–30°E). Moreover, the lidar of NASA airborne was flown on this day. These two data sets will be compared with the RADIBAL results.

3.2.1. *SAM II data.* SAM II measures the extinction of the solar irradiance at λ = 1020 nm for the slant path at a tangent altitude z. After removing the residual Rayleigh optical thickness, the aerosol slant optical thicknesses are inverted to provide a vertical profile of the aerosol extinction coefficient. The nine recorded aerosol vertical profiles

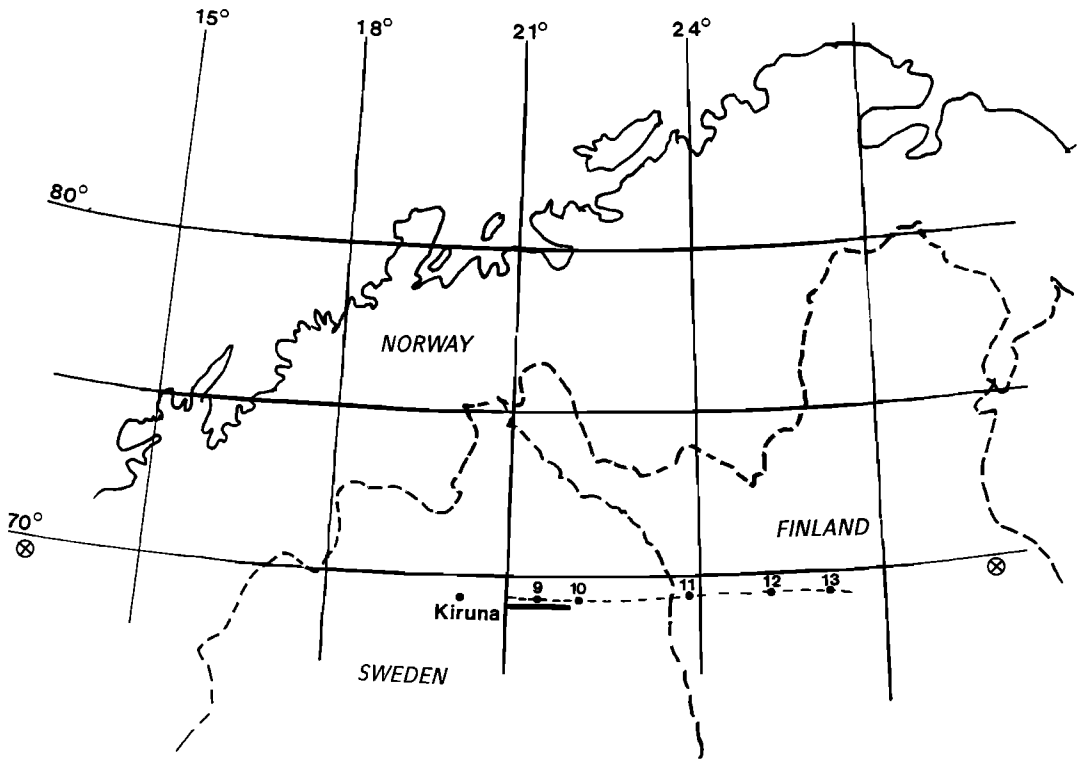

Fig. 12. Map of Scandinavia with the locations of the joint experiments on January 28, 1988. SAM II tangent points are indicated by circled crosses. The balloon was launched from Kiruna, and the dashed line represents the trajectory labeled with time every hour. The solid line corresponds to the part of the NASA DC8 trajectory where the lidar was running.

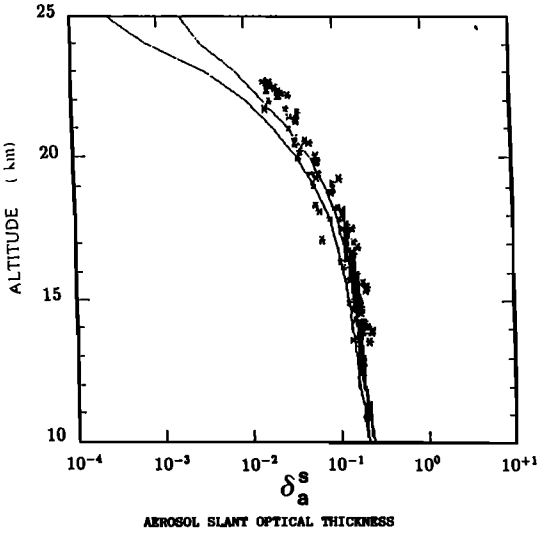

Fig. 14. Comparison of the aerosol slant optical thicknesses at λ = 1020 nm between RADIBAL (stars) and SAM II (limit, solid lines).

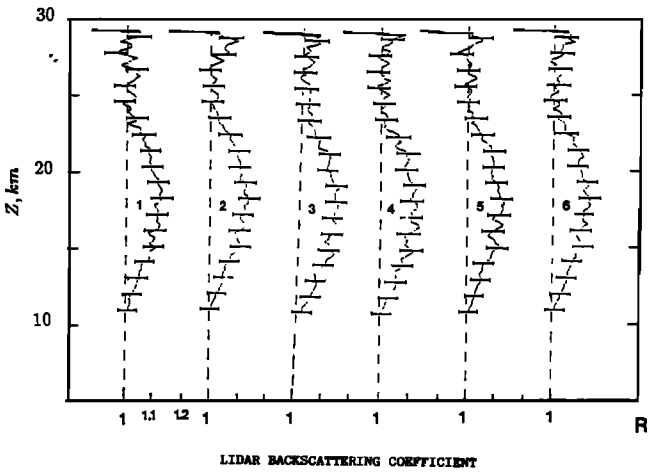

Fig. 15. Lidar backscattering ratio versus altitude at 532 nm measured from the NASA DC8 in Kiruna on January 28, 1988. The x scale is provided only for the first set, and the unit value for the other sets.

showed a quite stable aerosol layer. On a map of Scandinavia (Figure 12), we reported the two SAM events which bounded the RADIBAL trajectory. The SAM profile obtained at 0756 UT for a tangent point at (69.9°N, 28.3°E) is included in the error bars of the second profile obtained at 0936 UT for (69.9°N, 13.8°E) (Figure 13). This winter was mild, and no PSC were recorded. Moreover, the air masses were confined and isolated in the vortex. We then had a very stable and homogeneous situation.

The comparison with RADIBAL is done in Figure 14. The RADIBAL measurements confirmed the spatial homogeneity up to 22-km altitude, where the Junge layer is vanishing. Along the profile probed (between 200 hPa and 35 hPa), the hydrated sulfuric acid aerosol particles are quite stable with an effective radius of $r_{\text{eff}} = 0.33 \pm 0.02$ μm for an effective variance of $v_{\text{eff}} = 0.10 \pm 0.02$. The RADIBAL slant optical thicknesses at 1020 nm are computed using the spectral dependence of the inverted model deduced from the 1650-nm slant optical thickness measurements. The two solid-line curves correspond to the extreme SAM data obtained when taking into account the error bars. The SAM upper values closely match the RADIBAL results.

3.2.2. *Lidar measurements.* During CHEOPS, PSC observations were performed by a lidar (λ = 532 nm) set up on the NASA aircraft. Description of the apparatus is reported in *Osborn et al.* [1989]. A joint flight with the RADIBAL experiment also occurred on January 28, 1988. Table 2 gives the conditions of the lidar measurements, and Figure 15 reports the backscattering ratio derived from the lidar data:

$$R = \frac{\sigma_a p_a + 1.5\sigma_R}{1.5\sigma_R} \tag{12}$$

where p_a is the aerosol phase function in backscattering; R is normalized at an altitude of 24 km assuming that the aerosol abundance is quite null at this altitude, R being a function of altitude; and σ_R is proportional to the barometric pressure and depends upon the temperature. Radiosondes are used to derive the P-T vertical profile, and R can then be converted into an aerosol backscattering coefficient:

$$b_a = \frac{\sigma_a p_a}{4\pi} \tag{13}$$

To compare with RADIBAL, we need to integrate the lidar data over the slant path. We compute then a slant backscattering coefficient B_a for the lidar measurements as

$$B_a^L(z) = \sqrt{R/2} \int_0^\infty \frac{b_a(z')}{\sqrt{z' - z}}\, dz' \tag{14}$$

Using the lognormal distribution deduced from the RADIBAL measurements, the aerosol phase function p_a at $\Theta = 180°$ is computed at 532 nm. In the same way, using the spectral dependence of the model, the aerosol slant optical thickness is deduced at 532 nm from the 1650-nm measurements. The result is a slant backscattering coefficient:

$$B_a(z) = \frac{\delta_a^s(z) p_a}{4\pi} \tag{15}$$

The comparison is reported in Figure 16. The y axis is given in barometric pressure, which corresponds to the balloon measurements, while lidar data pressure originated from a conversion of altitude to pressure using the nearest available radiosonde. This presentation indicates that a difference in pressure of few hectopascals may result in the

TABLE 2. Conditions of the Lidar Measurements

	Profile					
	1	2	3	4	5	6
Start time, UT	1434	1445	1459	1512	1522	1530
End time, UT	1442	1457	1509	1521	1528	1539
Latitude N	67.7	67.7	68.2	68.1	67.9	67.8
	−67.7	68.3	68.1	67.9	67.8	68.0
Longitude E	21.3	23.0	21.6	21.5	22.8	22.7
	22.6	21.6	21.2	22.7	22.9	21.5

Latitudes and longitudes are shown as the range during the profile.

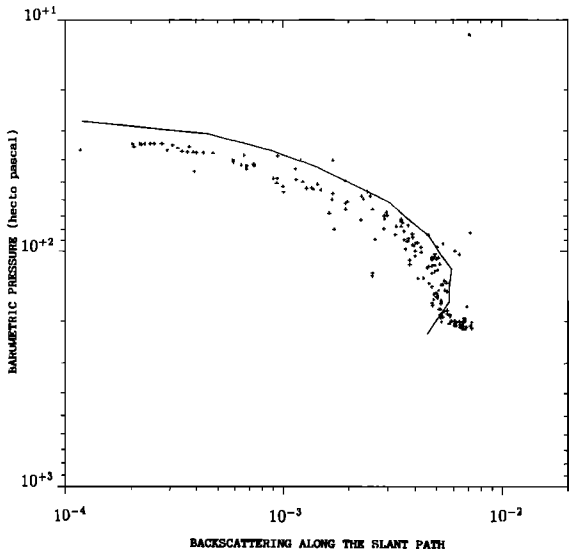

Fig. 16. Comparison of the lidar slant backscattering coefficient (solid line) to the RADIBAL-deduced values (crosses).

observed systematic bias. In the main layer, the agreement is achieved within 30%. The discrepancies at the lower altitudes result from RADIBAL inaccuracies. These points correspond to sun position below the horizon, and the atmospheric transmittances are difficult to estimate. Above the layer the behaviors of the two data sets are identical.

4. Conclusions

We first adapted the RADIBAL inversion scheme to suit the descending flight, and we applied this strategy to the May 13, 1984, and to the January 28, 1988, measurements.

The analysis of the RADIBAL measurements is quite coherent with those based on polarization measurements done at Le Pic du Midi. That indicates that the modelization of the signal in the spherical atmosphere of RADIBAL fits a more simple approach in a plane-parallel atmosphere at Le Pic du Midi. Moreover, the availability of complementary measurements on the ground-based station, such as multispectral extinction measurements or aureole measurements, offered an opportunity to verify the ability of the RADIBAL inverted model to retrieve the main optical properties of the medium.

The last section has shown the comparison of various measurements of the extinction coefficient, such as limb photography, occultation measurements, and lidar measurements, with RADIBAL predictions when the spatiotemporal coincidence is suitable. The good agreement proves RADIBAL to be a good candidate to validate SAGE II products, and a future work will deal with this problem.

Acknowledgments. The RADIBAL experiment benefited from the technical support of P. Lecomte, L. Gonzalez, and C. Verwaerde. We acknowledge the CNES balloon division for technical assistance as well as the IASB team, which supported the limb experiment. C. Deaux and P. Lecomte collected the ground-based data at Le Pic du Midi. We acknowledge C. Lenoble and P. McCormick for providing SAM and lidar data. The work done at LOA has been supported by the French Comité Atmosphere Moyenne.

References

Ackerman, M., C. Lippens, and C. Muller, Stratospheric aerosol prospectives from Earth limb photography, *Nature, 292*, 587–591, 1981.

Deuzé, J. L., M. Herman, and R. Santer, Fourier series expansion of the transfer equation in the atmosphere-ocean system, *J. Quant. Spectrosc. Radiat. Transfer, 41*(6), 483–494, 1989.

Devaux, C., M. Herman, R. Santer, and D. Tanré, On the complementarity of solar transmission and aureola measurements to derive the aerosol size distribution: Application to desert aerosol characteristic retrievals, in *Proceedings of the International Radiation Symposium*, edited by J. Lenoble and D. Geleyn, pp. 557–560, A. Deepak, Hampton, Va., 1989.

Hansen, J. E., and L. D. Travis, Light scattering in planetary atmospheres, *Space Sci. Rev., 16*, 527, 1974.

Herman, M., J. Y. Balois, L. Gonzalez, P. Lecomte, J. Lenoble, R. Santer, and C. Verwaerde, Stratospheric aerosol observations from a balloon-borne polarimetric experiment, *Appl. Opt., 25*, 3573–3584, 1986.

King, M. D., D. M. Byrne, B. M. Herman, and J. A. Reagan, Aerosol size distributions obtained by inversion of spectral optical depth measurements, *J. Atmos. Sci., 35*, 2153–2167, 1978.

Osborn, M. T., J. M. Rosen, M. P. McCormick, P.-H. Wang, J. M. Livingston, and T. J. Swissler, SAGE II aerosol correlative observations: Profile measurements, *J. Geophys. Res., 94*(D6), 8353–8366, 1989.

Santer, R., and M. Herman, Particle size distributions from forward scattered light using the Chahine inversion scheme, *Appl. Opt., 22*(15), 2294–2301, 1983.

Santer, R., M. Herman, D. Tanré, and J. Lenoble, Characterization of the stratospheric aerosol polarization measurements, *J. Geophys. Res., 93*, 14,209–14,221, 1988.

Weinman, J. A., J. T. Twitty, S. R. Browing, and B. M. Herman, Derivation of phase functions from multiply scattered sunlight transmitted through a hazy atmosphere, *J. Atmos. Sci., 32*, 577–583, 1975.

C. Brogniez, S. Diallo, M. Herman, and R. Santer, Laboratoire d'Optique Atmosphérique, Université des Sciences et Technologies de Lille, 59655 Villeneuve d'Ascq cedex, France.

M. Ackerman, Institut d'Aeronomie Spatiale de Belgique, Brussels, Belgium.

(Received January 3, 1992;
revised July 21, 1992;
accepted August 20, 1992.)